energies

MDPI

Article

A Method for State of Charge and State of Health Estimation of Lithium Batteries Based on an Adaptive Weighting Unscented Kalman Filter

Fengyuan Fang, Caiqing Ma * and Yan Ji

College of Automation and Electronic Engineering, Qingdao University of Science and Technology, Qingdao 266061, China; 4021040010@mails.qust.edu.cn (F.F.); yjichina@163.com (Y.J.)
* Correspondence: mcqqqd@163.com

Abstract: This paper considers the estimation of SOC and SOH for lithium batteries using multi-innovation Levenberg–Marquardt and adaptive weighting unscented Kalman filter algorithms. For parameter identification, the second-order derivative of the objective function to optimize the traditional gradient descent algorithm is used. For SOC estimation, an adaptive weighting unscented Kalman filter algorithm is proposed to deal with the nonlinear update problem of the mean and covariance, which can substantially improve the estimation accuracy of the internal state of the lithium battery. Compared with fixed weights in the traditional unscented Kalman filtering algorithm, this algorithm adaptively adjusts the weights according to the state and measured values to improve the state estimation update accuracy. Finally, according to simulations, the errors of this algorithm are all lower than 1.63 %, which confirms the effectiveness of this algorithm.

Keywords: multi-innovation Levenberg–Marquardt algorithm; adaptive weighting unscented Kalman filter; SOC estimation; SOH estimation

Citation: Fang, F.; Ma, C.; Ji, Y. A Method for State of Charge and State of Health Estimation of Lithium Batteries Based on an Adaptive Weighting Unscented Kalman Filter. *Energies* **2024**, *17*, 2145. https://doi.org/10.3390/en17092145

Academic Editors: King Jet Tseng, JongHoon Kim and Jeong-Hun Park

Received: 28 February 2024
Revised: 8 April 2024
Accepted: 22 April 2024
Published: 30 April 2024

1. Introduction

Lithium batteries have significant advantages, such as good safety performance, excellent discharge characteristics, and high energy density [1,2]. These qualities make them crucial to the future direction of energy production. To ensure high reliability and operational safety, the battery management system (BMS) must track and control the electrical system in real-time [3,4]. The state of charge (SOC) and state of health (SOH) are crucial factors in the BMS that influence the battery's energy management distribution. SOC refers to the current remaining charge of the battery, and its effective estimation is essential to the operating process of a lithium battery. SOH means the health of the lithium battery, usually expressed as resistance or capacity. In summary, the accuracy of SOC and SOH estimation helps to better manage and maintain a lithium battery, ensuring the safety and reliability of the battery [5,6].

Lithium battery models can be used to describe the electrical behavior and characteristics of the battery, which can enhance understanding of how lithium batteries work, facilitating prediction of the SOC and lifetime of lithium batteries. Currently, there are four prevalent types of battery models: electrochemical models [7–9], neural network models [10], alternating current (AC) impedance models [11,12], and the equivalent circuit model [13]. Compared with the AC impedance and electrochemical models, the equivalent circuit model can simplify the complex internal structure and improve computational efficiency. It can directly reflect the dynamic processes and state changes inside the battery. Compared to the neural network model, the equivalent circuit model has enhanced precision in predicting the SOC, the SOH, and the remaining useful life (RUL) based on known internal battery parameters [14,15], and black-box effects, and over-fitting can be avoided [16].

The open circuit voltage method is one of the most prevalent methods for estimating the SOC, but the results estimated by this method can be confounded by environmental factors and require a longer test time. Therefore, the method is generally not considered for practical applications. Zhang et al. proposed a particle filter in the battery SOC and the open circuit voltage (OCV) estimation, which can avoid the influence of noise generated during battery terminal voltage measurement and current drift [17]. The ampere-time integration method requires the use of high-precision test equipment to obtain accurate data. Moreover, the initial values are not easy to determine and this model is not suitable for rapid testing of the lithium battery state in a short period of time. Liu et al. linked the EKF and Ah-integral algorithms to apply the fuzzy-extended Kalman filter-ampere-hour algorithm. The serious estimation error in the strong nonlinear interval of the EKF algorithm and the accumulated error generated by the sampling accuracy of the ampere-time integration algorithm may both be successfully resolved by the fused algorithm [18]. Support vector machines are based on vectors to construct a decision boundary, so data interference has a more significant impact on them than other methods; therefore, it is important to ensure thorough data cleaning. Kim et al. utilized basic building blocks, such as the residual and leverage statistics, to represent the Cook distance, using simple descriptive statistics and approximation measures. They proposed application of the deletion method and the infinitesimal perturbation method to address outlier effects in vector machines [19]. The neural network has many parameters to identify, which can lead to a more complex network structure that is not easily optimized, moreover, the model itself is less interpretable. Talha et al. proposed a neural network (NN) simplified state estimation algorithm that can directly estimate the SOC and SOH online in the absence of the internal parameters of the battery. Finally, the reliability of this algorithm was demonstrated through experiments [20].

The model-based method offers higher flexibility compared to conventional and data-driven methods. Combining models and filters to estimate the SOC is a prevalent modeling method. Based on the dual-polarization model, Tan et al. proposed the EKF algorithm to calculate the SOC and SOP of lithium batteries. Simulations showed that the EKF algorithm can achieve high predictive values under any operating conditions, reflecting the effectiveness of this algorithm [21]. However, this method is not suitable for solving problems with special noise and unknown uncertainty. In order to solve the problem of low accuracy of the EKF algorithm, Li et al. proposed the forgetting factor stochastic gradient-multi-innovation extended Kalman filter (FFSG-MIEKF) algorithm for parameter identification and SOC estimation. Simulations were used to demonstrate the effectiveness of this algorithm [22]. However, the MIEKF algorithm introduces covariance matrix repair and an update operation, which increases the calculation required and the complexity of the algorithm. El Din et al., combining an unscented transform and Kalman filter using covariance estimation for the sampling point state noise and observation noise, proposed an unscented Kalman filter (UKF) to improve the state estimation accuracy. Finally, experiments were undertaken to confirm the effectiveness of this algorithm [23]. As the UKF algorithm needs to use sigma points, the amount of computation and the accuracy of calculation are affected during state estimation. In order to reduce the effect of interference on the SOC accuracy, in this paper, the mean and observation weights are adaptively adjusted according to the state and observation residual vectors so that this algorithm has better weight stability in state estimation.

The parameter estimation of battery models is very important for battery performance analysis and the parameters of battery models can be identified through some identification methods [24–29] from observation data such as the gradient-based algorithms [30–34] and the least squares-based identification methods [35–38]. In practical applications, the SOH plays a very important role in maintaining the performance and extending the life of a battery. Relatively speaking, the SOH and the internal resistance have a more direct link, so the internal resistance is chosen as the state variable for estimating the SOH [39–41]. In current research, most studies have considered the SOC and SOH separately, with the

interaction between them rarely considered in the process of estimating the state parameters of the battery. Consequently, we propose an adaptive weighting unscented Kalman filter algorithm (AWUKF) algorithm. This algorithm is based on the SOC for SOH estimation, and can greatly reduce the problem of decreased accuracy of state estimation caused by environmental changes. The main contributions of the paper are as follows:

- The AWUKF algorithm reselects the particles using the unscented transformation, and the adaptive weights are brought into the UKF framework to reduce the sensitivity to noise.
- This algorithm is utilized to attenuate the deviation of the SOC values under measurement and state noise disturbances; moreover, the SOC is used as a basis for estimating the SOH values.
- Simulations are carried out under different experimental conditions to assess the practicality and effectiveness of this algorithm.

The paper is organized as follows: Section 2 describes the circuit model of the lithium battery. The construction of the multi-innovation Levenberg–Marquardt (MILM) algorithm to determine the internal parameters of the battery is described. Section 3 considers the AWUKF algorithm, and uses this algorithm for joint estimation of the SOC and SOH. Section 4 subjects the traditional EKF, the UKF, and the AWUKF algorithms to experimental simulation under different experimental conditions. Finally, Section 5 summarizes the main conclusions and presents some perspectives.

2. Battery Model

2.1. Integral Second-Order RC Model

V_{ocv} is the open-circuit voltage, V_0 is the terminal voltage, and I is the load current. The first RC network describes the polarization characteristics, R_{p1} denotes the polarization resistance, and C_{p1} represents the polarization capacitance. The second RC circuit represents the dynamic behavior of the lithium battery related to the concentration polarization, R_{p2} represents the concentration polarization resistance, and C_{p2} represents the capacitance [42–44]. The second-order RC equivalent circuit model is shown in Figure 1.

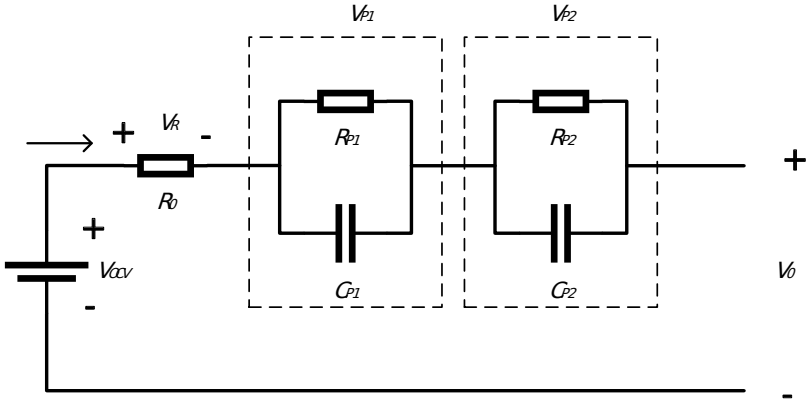

Figure 1. Circuit structure of the second-order RC equivalent circuit model.

The electrical characteristics of the model can be expressed as

$$\begin{aligned} V_0 &= V_{ocv} - V_R - V_{p1} - V_{p2}, \\ V_{p1} &= IR_{p1} - C_{p1}\frac{\mathrm{d}V_{p1}}{\mathrm{d}t}, \\ V_{p2} &= IR_{p2} - C_{p2}\frac{\mathrm{d}V_{p2}}{\mathrm{d}t}, \end{aligned}$$

where V_{p1} and V_{p2} are the terminal voltages of the $R_{p1}C_{p1}$ and $R_{p2}C_{p2}$ circuits, respectively.

By Laplace transformation, we get the electrical characteristic equation:

$$V_0(s) - V_{ocv}(s) = I(s)\left[R_0 + \frac{R_{p1}}{1 + C_{p1}R_{p1}s} + \frac{R_{p2}}{1 + C_{p2}R_{p2}s}\right]. \tag{1}$$

It follows the discretization expression:

$$\frac{V_0(s) - V_{ocv}(s)}{-I(s)} = \frac{R_0(1 + \tau_1 s)(1 + \tau_2 s) + R_{p1}(1 + \tau_2 s) + R_{p2}(1 + \tau_1 s)}{(1 + \tau_1 s)(1 + \tau_2 s)}. \tag{2}$$

Applying the bilinear transformation to (2), we get the differential equation for the system:

$$V_0(t) = \theta_1 V_0(t-1) + \theta_2 V_0(t-2) + \theta_3 I(t) + \theta_4 I(t-1) + \theta_5 I(t-2) + \theta_6, \tag{3}$$

where

$$\begin{cases} \theta_1 = -(\tau_1 + \tau_2), \\ \theta_2 = -\tau_1\tau_2, \\ \theta_3 = -(R_0 + R_{p1} + R_{p2}) \\ \theta_4 = -(R_0\tau_1 + R_0\tau_2 + R_{p1}\tau_2 + R_{p2}\tau_1), \\ \theta_5 = -R_0\tau_1\tau_2, \\ \theta_6 = (1 + \tau_1 + \tau_2 + \tau_1\tau_2)V_{ocv}, \end{cases} \tag{4}$$

where τ_1 and τ_2 represents the time constants, which can be obtained by $R_{p1}C_{p1}$ and $R_{p2}C_{p2}$, respectively. θ_1 to θ_6 are equivalent expressions of the correlation coefficients. The internal resistance R_0, the polarization resistors R_{p1} and R_{p2}, and the polarization capacitors C_{p1} and C_{p2} are obtained based on the measured data. Then, the optimization algorithm is used to identify θ_i $(i = 1, 2, 3, 4, 5, 6)$. The parameter optimization algorithm is described in detail in the next section. The proposed parameter estimation algorithms in this paper are based on the identification model in (3). Many identification methods are derived based on the identification models of the systems [45–49] and these methods can be used to estimate the parameters of other linear systems and nonlinear systems [50–54] and can be applied to other fields [55–59] such as chemical process control systems.

2.2. Parameter Identification Based on MILM Method

The traditional LM algorithm combines gradient descent insensitivity to initial values and Gaussian–Newton global optimality characteristics. Based on this property, the solution efficiency of the LM algorithm in between the two methods can be determined [60]. Therefore, based on multi-innovation theory, by extending a single innovation into a multi-innovation vector containing both past moment and current moment data, an MILM algorithm is proposed to improve the accuracy of battery parameter identification. The specific process used is as follows:

First, the recognition model is as follows:

$$V_0(t) = \varphi^{\mathrm{T}}(t)\theta + \nu(t), \tag{5}$$

where V_0 are the observed output data, $\varphi(t) = [V_0(t-1), V_0(t-2), I(t), I(t-1), I(t-2), 1]^{\mathrm{T}}$ is composed of the terminal voltage and current input data, $\theta = [\theta_1, \theta_2, \theta_3, \theta_4, \theta_5, \theta_6]^{\mathrm{T}}$ is the parameter vector to be identified, and $\nu(t)$ is zero mean random noise.

According to the LM algorithm, the quadratic criterion function for the nonlinear system is given by

$$J(\theta) = \frac{1}{2}\|V_0(t) - \varphi^{\mathrm{T}}(t)\theta\|^2. \tag{6}$$

According to (5) and (6), the first-order partial derivative and the second-order partial derivative of $J(\theta)$ with respect to θ are defined as

$$\nabla J(\theta) = \frac{\partial J(\theta)}{\partial \theta} = -\varphi^{\mathrm{T}}(t)\nu(t), \tag{7}$$

$$H(\theta) = \frac{\partial^2 J(\theta)}{\partial \theta \partial \theta^{\mathrm{T}}} = \varphi(t)\varphi^{\mathrm{T}}(t), \tag{8}$$

According to (7) and (8), the introduction of the damping factor μ decreases the sensitivity to the initial values problem and enables the Gaussian–Newton characteristics to converge quickly around the optimum. Thus, we can obtain the LM algorithm:

$$\hat{\theta}(t) = \hat{\theta}(t-1) - [H(\hat{\theta}(t)) + \mu I]^{-1} \nabla J(\hat{\theta}(t)).$$

Using the multi-innovation identification theory [61–68], the single innovation is expanded into multi-innovation:

$$\nu(t) = V_0(t) - \varphi^{\mathrm{T}}(t)\theta, \tag{9}$$

$$\nu(p,t) = \begin{bmatrix} \nu(t) \\ \nu(t-1) \\ \cdots \\ \nu(t-p+1) \end{bmatrix} = \begin{bmatrix} V_0(t) - \varphi^{\mathrm{T}}(t)\theta \\ V_0(t-1) - \varphi^{\mathrm{T}}(t-1)\theta \\ \cdots \\ V_0(t-1) - \varphi^{\mathrm{T}}(t-1)\theta \end{bmatrix}, \tag{10}$$

where p is the innovation length.

The input data matrix $\Phi(p,t)$ and output terminal voltage vector $V_0(p,t)$ are defined as

$$\Phi(p,t) = [\varphi(t), \quad \varphi(t-1), \quad \cdots \quad , \quad \varphi(t-p+1)]^{\mathrm{T}}, \tag{11}$$

$$V_0(p,t) = [V_0(t), \quad V_0(t-1), \quad \cdots \quad , \quad V_0(t-p+1)]^{\mathrm{T}}. \tag{12}$$

Combining (9)–(12), the multi-innovation vector can be expressed as

$$\nu(p,t) = V_0(p,t) - \Phi^{\mathrm{T}}(p,t)\hat{\theta}(t-1), \tag{13}$$

where the state $\nu(p,t)$ is optimized by expanding $V_0(t)$ to $V_0(p,t)$ and $\varphi(t)$ to $\Phi(p,t)$. Therefore, the MILM algorithm can capture more information, and identifying the parameters is more accurate than for the LM algorithm.

In summary, the MILM algorithm is as follows:

$$\hat{\theta}(t) = \hat{\theta}(t-1) - [H(\hat{\theta}(t)) + \mu I]^{-1} \nabla J(\hat{\theta}(t)), \tag{14}$$

$$I = \mathrm{eye}(size(Q)), \quad Q = H(\hat{\theta}(t)), \tag{15}$$

$$\nabla J(\hat{\theta}(t)) = \frac{\partial J(\theta(t))}{\partial \theta} = -\Phi^{\mathrm{T}}(p,t)\nu(p,t), \tag{16}$$

$$H(\hat{\theta}(t)) = \frac{\partial^2 J(\theta(t))}{\partial^2 \theta} = \Phi(p,t)\Phi^{\mathrm{T}}(p,t). \tag{17}$$

3. The SOC and SOH Estimation Method

3.1. SOC Estimation Based on the AWUKF Algorithm

This paper proposes an adaptive weight method to adjust the system noise and measurement noise. Compared with the fixed weight in traditional UKF, the method adaptively adjusts the state estimation weight based on the state and measurement residual vector, which can improve the SOC estimate accuracy and convergence.

From the battery model, the state relationship equation is defined as

$$\begin{cases} \dot{x} = Ax + BI, \\ y = Cx + DI, \end{cases}$$

where

$$
\begin{aligned}
A &= \begin{bmatrix} 1 & 0 & 0 \\ 0 & \mathrm{e}^{-\alpha} & 0 \\ 0 & 0 & \mathrm{e}^{-\alpha} \end{bmatrix}, \\
B &= \begin{bmatrix} -\frac{\int_{t0}^{t} \eta \mathrm{d}t}{Q_N} \\ R_{p1} - R_{p1}\mathrm{e}^{-\alpha_1} \\ R_{p2} - R_{p2}\mathrm{e}^{-\alpha_2} \end{bmatrix}, \alpha_1 = \frac{\triangle\, t}{R_{p1}C_{p1}}, \alpha_2 = \frac{\triangle\, t}{R_{p2}C_{p2}}, \\
C &= [\frac{d_{ocv}}{d_{soc}} - 1 - 1], \quad D = -R_0, \\
x &= \begin{bmatrix} SOC \\ V_{p1} \\ V_{p2} \end{bmatrix}, \quad y = V_0, \quad x \in \mathbb{R}^3.
\end{aligned}
$$

The state equation and measurement equation are given by

$$
\begin{aligned}
x_{k+1} &= f(x_k, u_k) + \omega_k, \qquad (18) \\
y_{k+1} &= h(x_{k+1}, u_{k+1}) + v_k, \qquad (19)
\end{aligned}
$$

where $f(x_k, u_k)$ is the nonlinear state equation, $h(x_k, u_k)$ is the nonlinear measurement equation, u_k is the current, x_k is the state variable, subscript k denotes the kth discrete sampling, ω_k is the state noise, and v_k is the measurement noise. According to (18) and (19), the calculation process of the AWUKF algorithm is as follows.

The first values of the state and the error covariance matrix are given by

$$
\begin{aligned}
\hat{x}_0 &= \mathrm{E}[(x_0)], \\
P_0 &= \mathrm{E}[(x_0 - \hat{x}_0)(x_0 - \hat{x}_0)^{\mathrm{T}}].
\end{aligned}
$$

Select $2n + 1$ sample points:

$$
\begin{cases}
x_{k-1}^0 = \hat{x}_{k-1}, \\
x_{k-1}^{(i)} = \hat{x}_{k-1} + (\sqrt{(n+\lambda)P_{k-1}}),\ i = 1, 2, \cdots, L, \\
x_{k-1}^{(i)} = \hat{x}_{k-1} - (\sqrt{(n+\lambda)P_{k-1}}),\ i = L, L+2, \cdots, 2L,
\end{cases} \qquad (20)
$$

where i is the number of sample points.

Calculation of the weights coefficient:

$$
\begin{cases}
\lambda = \alpha^2(n + \kappa) - n, \\
\omega_c^{(0)} = \frac{\lambda}{n+\lambda}, \omega_c^{(i)} = \frac{\lambda}{2(n+\lambda)},\ i = 1, 2, \cdots, 2L, \\
\omega_m^{(0)} = \frac{1}{n+\lambda} + 1 - \alpha^2 + \beta, \omega_m^{(i)} = \frac{1}{2(n+\lambda)},\ i = 1, L+1, \cdots, 2L,
\end{cases} \qquad (21)
$$

where λ is a scaling coefficient, κ is an optional parameter, ω_m is the weighted value of the particle mean value, ω_c is the weighted value of the particle variance, and subscript i represents the ith discrete sampling. In the traditional algorithm, the weighting coefficient is a fixed value, but in practical applications, both the measurement noise and the state noise are random, being easily affected by temperature, voltage, and other factors. Therefore, an adaptive weights coefficient is proposed to adjust the state noise and the measurement noise.

Using (18), (20) and (21), the a priori state values and state covariance matrix for the $2n+1$ sample points are denoted by

$$x_{k|k-1}^{(i)} = f(x_{k-1}^{(i)}, u_{k-1}), i = 0, 1, 2, \cdots, 2L, \tag{22}$$

$$\hat{x}_{k|k-1} = \sum_{i=1}^{M} \omega_m^{(i)} x_{k|k-1}^{(i)}, \tag{23}$$

$$P_{k|k-1} = \sum_{i=1}^{M} \omega_c^{(i)} (\hat{x}_{k|k-1} - x_{k|k-1}^{(i)})(\hat{x}_{k|k-1} - x_{k|k-1}^{(i)})^{\mathrm{T}} + Q_{k-1}, \tag{24}$$

where the system noise covariance matrix uses Q_{k-1} at moment $k-1$.

According to the one-step predicted values in (23) and (24), the new sampling points are produced by the unscented transform:

$$x_{k|k-1}^{(i)} = [\hat{x}_{k|k-1}, \hat{x}_{k|k-1} + \sqrt{(n+\lambda)P_{k|k-1}}, \hat{x}_{k|k-1} - \sqrt{(n+\lambda)P_{k|k-1}}]. \tag{25}$$

Combining (19) and (25), the mean values and covariance matrix of the predicted observation are obtained by the weighted summation:

$$y_{k|k-1}^{(i)} = h(x_{k|k-1}^{(i)}, u_k), i = 0, 1, 2, \cdots, 2L, \tag{26}$$

$$\hat{y}_{k|k-1} = \sum_{i=1}^{M} \omega_m^{(i)} y_{k|k-1}^{(i)}, \tag{27}$$

$$P_{(\hat{y}_k, \hat{y}_k)} = \sum_{i=1}^{M} \omega_c{}^{(i)} (\hat{y}_{k|k-1} - y_{k|k-1}^{(i)})(\hat{y}_{k|k-1} - y_{k|k-1}^{(i)})^{\mathrm{T}} + R_k, \tag{28}$$

$$P_{(\hat{x}_k, \hat{y}_k)} = \sum_{i=1}^{M} \omega_c{}^{(i)} (\hat{x}_{k|k-1} - x_{k|k-1}^{(i)})(\hat{y}_{k|k-1} - y_{k|k-1}^{(i)})^{\mathrm{T}}, \tag{29}$$

where $P_{(y_k, y_k)}$ is the predicted measurement covariance matrix, $P_{(x_k, y_k)}$ is the state and measurement cross-covariance matrix, and R_k is the observation noise covariance matrix at moment k.

According to (28) and (29), update the Kalman gain by

$$K_k = P_{(\hat{x}_k, \hat{y}_k)} P_{(\hat{y}_k, \hat{y}_k)}^{-1}. \tag{30}$$

Use (23), (24), (27) and (30) to update the system state vector and covariance matrix:

$$\begin{aligned} \hat{x}_k &= \hat{x}_{k|k-1} + K_k(y_k - \hat{y}_{k|k-1}), \\ P_{k|k} &= P_{k|k-1} - K_k P_{(\hat{y}_k, \hat{y}_k)} K_k^{\mathrm{T}}. \end{aligned}$$

Adaptive weights are given by

$$\begin{cases} \Delta x_j = x_k - \hat{x}_{k|k-1}, \\ \Delta y_j = y_k - \hat{y}_{k|k-1}, \\ \|\Delta x_j\| = \sqrt{\Delta x_j^{\mathrm{T}} \Delta x_j}, \\ \|\Delta y_j\| = \sqrt{\Delta y_j^{\mathrm{T}} \Delta y_j}, \\ \lambda_j = \|\Delta x_j\| \|\Delta y_j\|, \\ \omega_j = \frac{\lambda_j}{\sum_{k=0}^{2L} \|\Delta x_j\| \|\Delta y_j\|}, \\ \omega_j = \omega_m^{(i)} = \omega_c^{(i)}, j = 1, 2, 3, \cdots, 2L. \end{cases}$$

3.2. SOH Estimation

The SOH of a lithium battery degrades over time until it can no longer meet the power and energy requirements. So, we need to predict the SOH of lithium batteries to ensure their safety and reliability. With increase in the number of charge and discharge cycles, a lithium battery will inevitably degrade. Therefore, the SOH of a battery can be indirectly computed using the ohmic internal resistance and the maximum available capacity.

Based on the SOH estimation of the ohmic internal resistance, the state of charge and V_{ocv} of the battery are taken as known values, and the state space equation of the system is established as

$$R_0(k+1) = R_0(k) + r(k), k = 1, 2, 3, \cdots, 2L, \tag{31}$$

where r is the process noise of the system, the mean is 0, and the covariance is σ_r.

The observation equation is as follows:

$$V_0(k) = V_{ocv}(k) - I(k)R_0(k) - V_{p1} - V_{p2} + \varepsilon(k), \tag{32}$$

where ε is the observed noise of the system, the mean value is 0, and the covariance is σ_ε.

According to (31) and (32), define the state relationship:

$$x_1(k+1|t) = x_1(k) + r(k), \tag{33}$$

$$y_1(k) = Ex_1(k) + F + \varepsilon(k), \tag{34}$$

where $E = -I(k)$ and $F = V_{ocv}(t) - V_{p1} - V_{p2}$. The SOC and SOH estimation algorithm proposed in this paper can combine some estimation algorithms [69–72] for studying new methods for linear and nonlinear stochastic systems with colored noises [73–77] and can be applied to other literatures such as industrial control systems [78–82], the information processing and communication systems and so on.

4. Simulation Experiment

4.1. Experimental Condition

When utilizing the MILM-AWUKF algorithm for lithium battery parameter identification and state estimation, it is necessary to construct a test platform for experimentation. This platform consists of a programmable temperature chamber, a battery operated device, and a computing machine. The subject is a lithium battery. The battery specifications are shown in Table 1.

Table 1. Battery information.

Information	Type	Data
Rate	Voltage	3.2 V
Operation	Voltage	2.7 V–4.2 V
Capacitance		3600 mAh
Rate	Charge current	0.72 A
Max	Discharge current	3.6 A

This paper uses the standard constant-current-constant-voltage charging and discharging mode, presenting a nonlinear relationship curve between SOC and OCV. Using sixth-order fit, the SOC-OCV fitting curve is presented in Figure 2 and the fitting equation in (35).

$$\begin{aligned} V_{ocv}(SOC) = {} & 6.4291 * SOC^6 - 14.0566 * SOC^5 + 9.0118 * SOC^4 - 0.5504 * SOC^3 \\ & - 0.9967 * SOC^2 + 0.8016 * SOC^1 + 3.5414. \end{aligned} \tag{35}$$

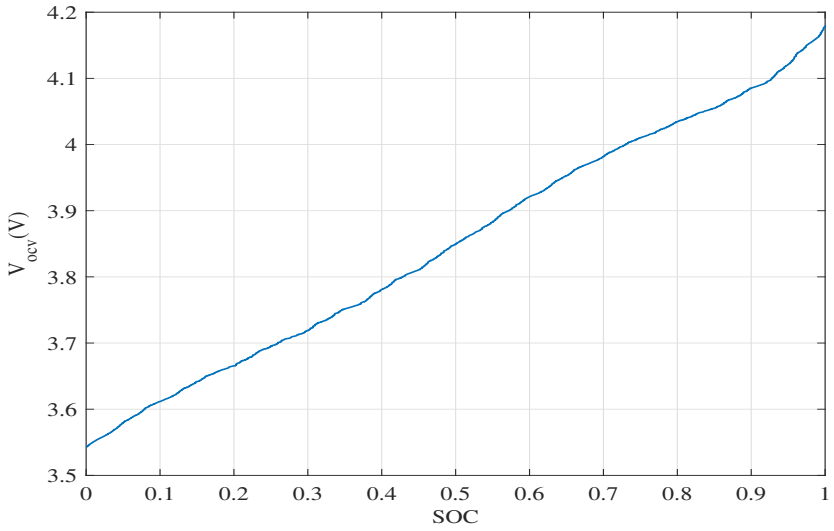

Figure 2. The experimental OCV-SOC curve.

4.2. Battery Parameters Identification Results

According to the second-order RC equivalent circuit model, the MILM algorithm is used to identify the resistance and capacitance parameters of the equivalent circuit model. The parameter identification results are shown in the figure. Figure 3 shows the MILM parameter identification under the federal urban driving schedule (FUDS). The results show that the parameter identification values converge quickly to stable values at a count of 112 and fluctuate within a small error range. Figure 4 shows the predicted and true values of the terminal voltage. It is clear that the predicted values of the terminal voltage closely follow the true values, with root mean square error (RMSE) values of about 0.0606% and mean absolute error (MAE) values of about 0.0345%. Figure 5 shows that the terminal voltage error range is consistently within 0.5%, indicating that this algorithm can characterize the dynamic characteristics and internal parameters of the battery model very well.

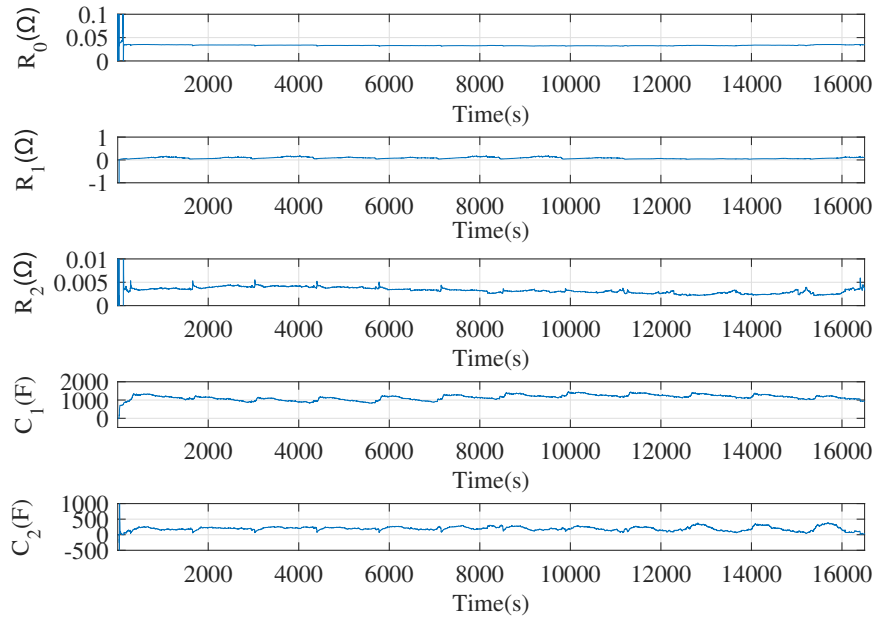

Figure 3. Results of MILM parameter identification under FUDS.

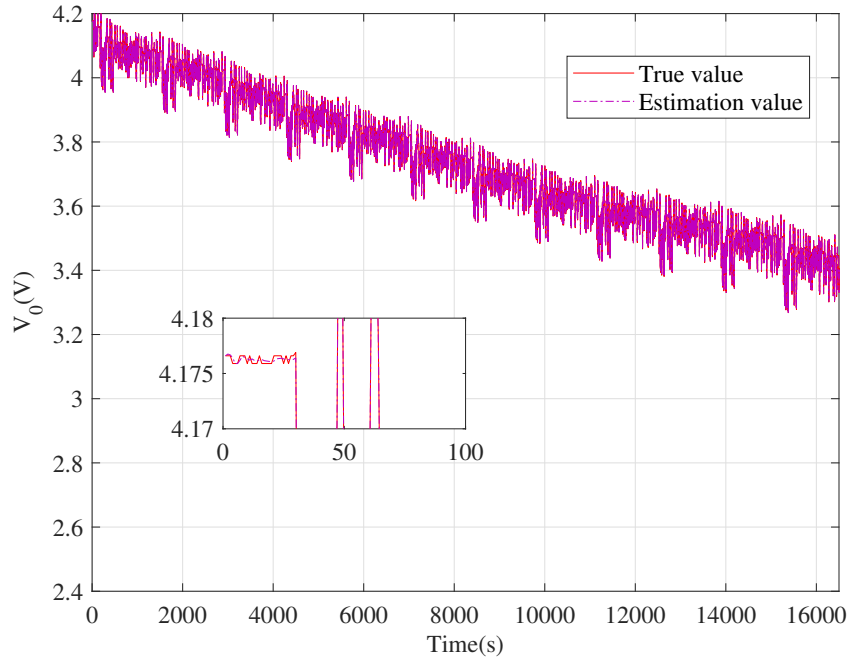

Figure 4. Results of voltage under FUDS.

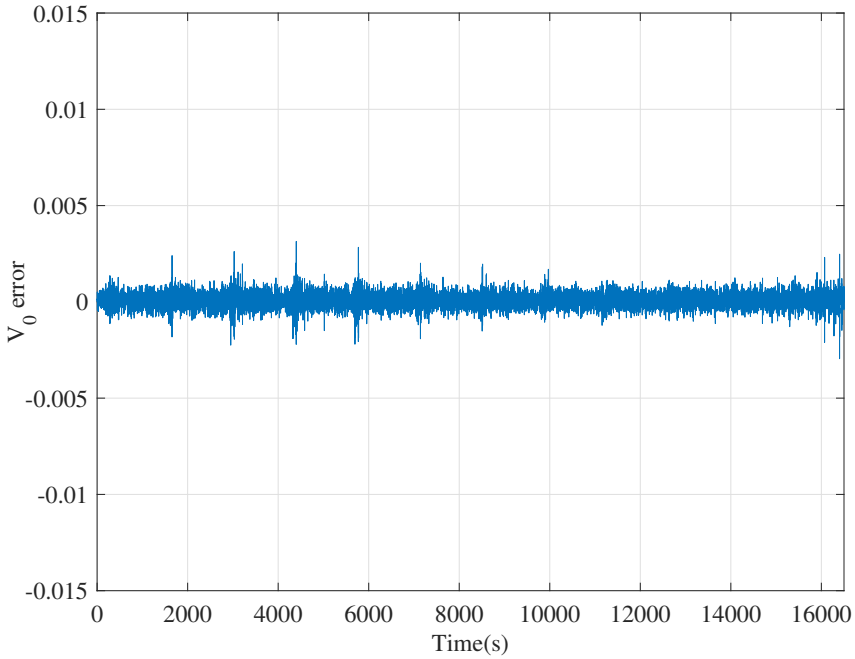

Figure 5. Results of voltage error under FUDS.

Figure 6 shows the MILM parameter identification results under dynamic stress testing (DST). Unlike the FUDS experiment, the equivalent model parameter identification results are not smooth and exhibit relatively large fluctuation except for R_0. The equation of each parameter is derived from (4), which is associated with the characteristics of the input voltage and current under the DST experiment. We infer from these results that the voltage and current do not vary at most moments and the voltage and current values are too large at a certain moment.

However, from subsequent comparison of the predicted and true values of the terminal voltage, we conclude that the errors obtained when using this algorithm are still very small

under complex conditions, verifying the reliability and safety of this algorithm.

Figures 7 and 8 present the predicted values and errors of the terminal voltages during DST. The predicted values of the terminal voltages converge to the true values at 187 sampling periods, with an error of about 0.015%, which represents a small range of change. In summary, even though the fluctuation in the identification parameters is large under current shock, it can be seen from the RMSE value of 0.012% and the MAE value of 0.002758% that there is minimal deviation between the predicted and true values of the voltages, which enables us to rely on these predictions with more confidence for the SOC and SOH estimation decisions. This accurate estimation can improve the system's understanding of the battery state, thus enhancing the performance and efficiency of the battery management system, reflecting the algorithm's excellent performance in modeling and predicting complex systems.

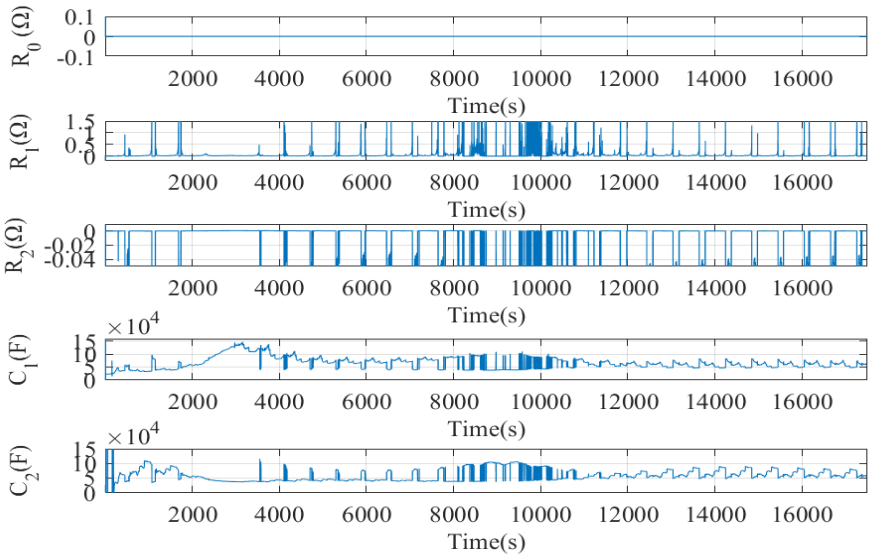

Figure 6. Results of MILM parameter identification under DST.

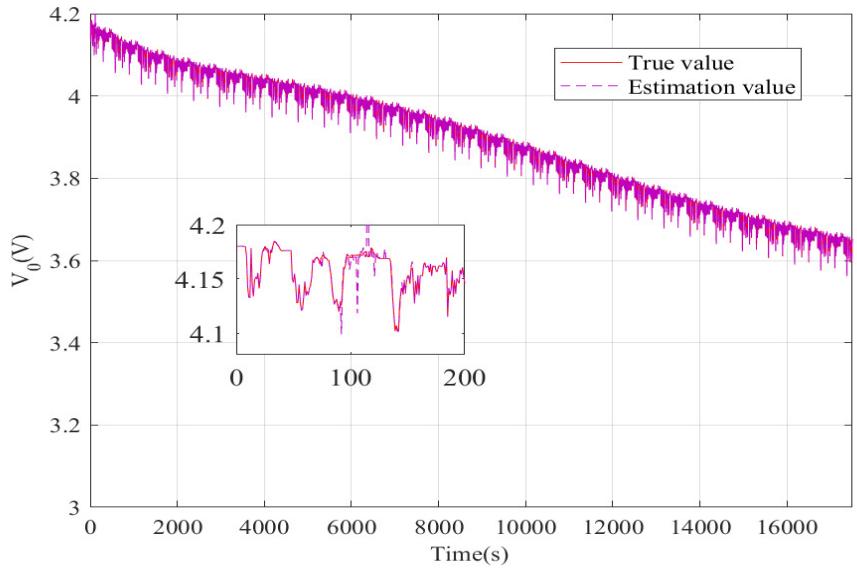

Figure 7. Results of voltage under DST.

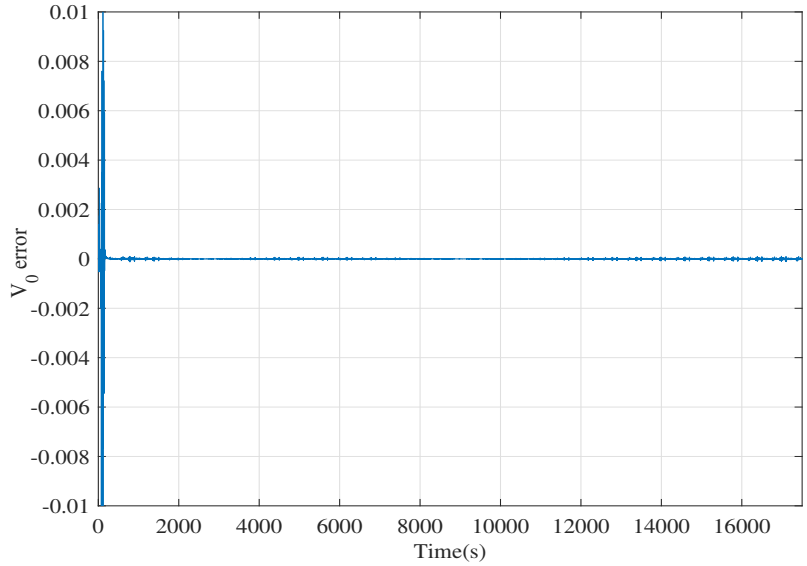

Figure 8. Results of voltage error under DST.

4.3. SOC Prediction Results

First, the initial values of SOC are set to 0.93. From Figures 9 and 10, with regard to the convergence speed and accuracy, it can be concluded that the EKF has the worst estimation performance, the AWUKF algorithm is better, and the UKF algorithm performance is between these two algorithms. In terms of SOC prediction, the SOC estimated by the AWUKF algorithm overlaps with the true values after 217 cycles in the battery state retention time interval, and the SOC estimated by the UKF algorithm overlaps with the true value for the first time after 662 cycles. In terms of error, After 106 cycles, the error of the AWUKF algorithm remains at about 0.1% and the error of the UKF algorithm remains within 3.5%. The SOC estimation accuracy under the DST experimental conditions shows that the proposed algorithm can not only improve the dynamic performance, but can also increase the estimation convergence speed.

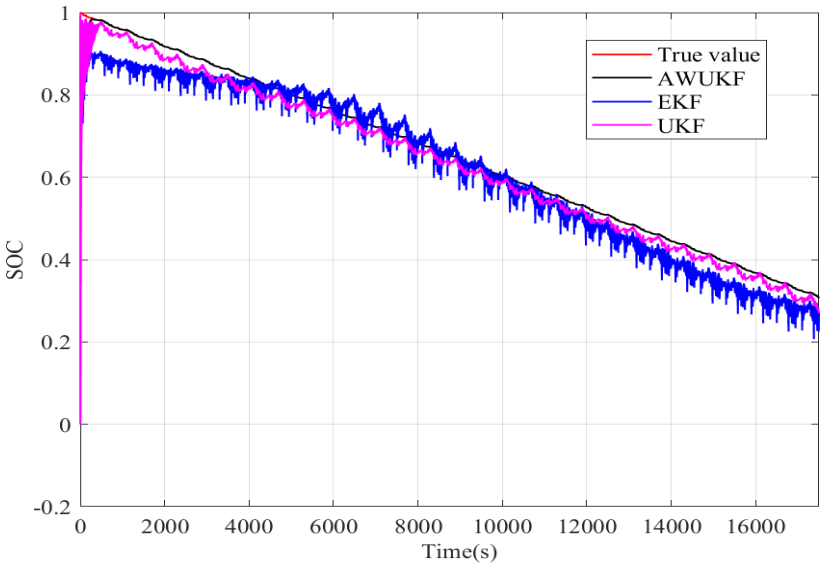

Figure 9. SOC estimation under DST test.

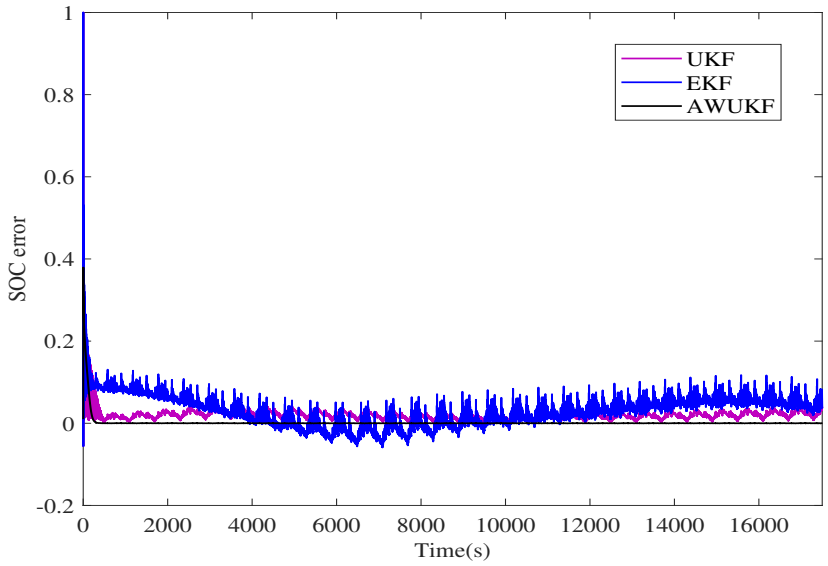

Figure 10. SOC estimation error under DST test.

The two indicators RMSE and MAE are used for evaluation. As shown in Table 2, the values of RMSE and MAE for the AWUKF algorithm are about 1%. Therefore, the estimation error can be greatly reduced by using this algorithm for state estimation.

Table 2. SOC estimation results under DST conditions.

	RMSE	**MAE**
AWUKF	0.0133	0.0011
UKF	0.0299	0.0211
EKF	0.0442	0.0350

Firstly, the initial values of SOC are set to 0.95; then, the EKF, UKF, and AWUKF algorithms are used to estimate the SOC under FUDS experimental conditions. Figure 11 shows the SOC prediction results using the different algorithms. It can be seen that the curves of the AWUKF and UKF algorithms are closest to the true values. However, with delay in time, compared to the UKF algorithm, the AWUKF algorithm can track the actual values well. Figure 12 shows the error curves for the different algorithms. It is clear that the UKF algorithm has an increasing error, while the AWUKF algorithm error becomes smaller and smaller, with a maximum error of about 2.5% after 5000 cycles. This confirms the accuracy and convergence of this algorithm.

As can be seen from Table 3, using RMSE and MAE to evaluate SOC estimation errors, the AWUKF algorithm has the smallest error among the three algorithms. This indicates that this model has good predictive ability for SOC estimation of lithium batteries.

Table 3. SOC estimation results under FUDS conditions.

	RMSE	**MAE**
AWUKF	0.0285	0.0188
UKF	0.0584	0.0324
EKF	0.0907	0.0774

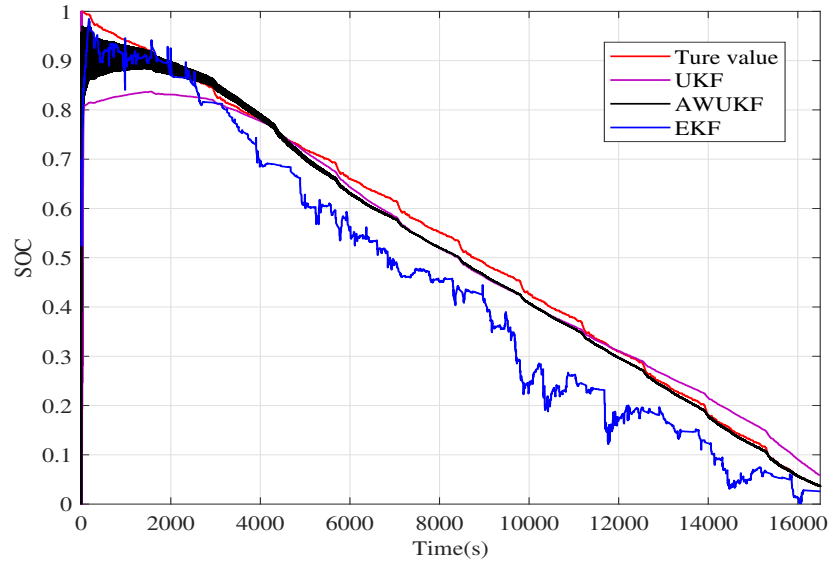

Figure 11. SOC estimation under FUDS test.

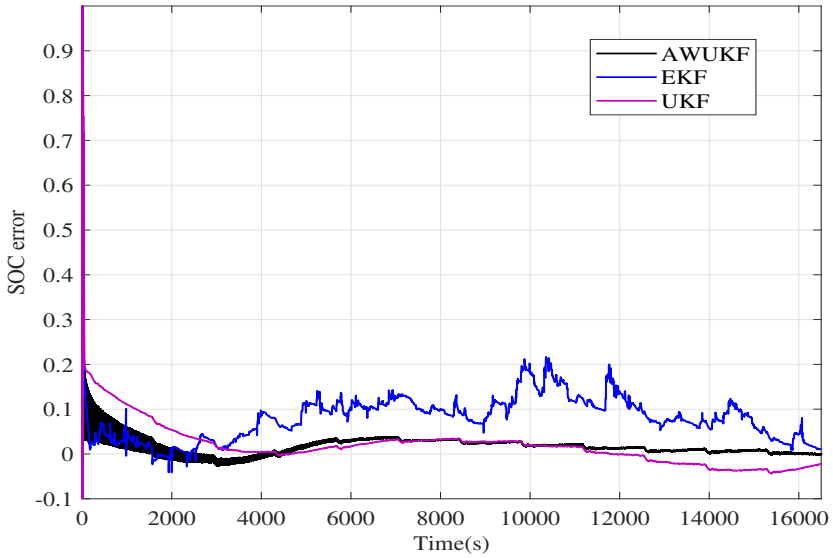

Figure 12. SOC estimation error under FUDS test.

4.4. SOH Prediction Results

Combining (33) and (34), using the EKF, UKF, and AWUKF algorithms to calculate the internal resistance. From Figures 13 and 14, it can be seen that the EKF algorithm provides the worst estimation curve. The estimation curves of the UKF and AWUKF algorithms are very close. Because the resistor itself is small, as can be seen by examination of the local zoomed-in image, the AWUKF algorithm is closer to the true value. It is clear from the error curves that the AWUKF algorithm quickly converges to a range close to the true values, and the error decreases.

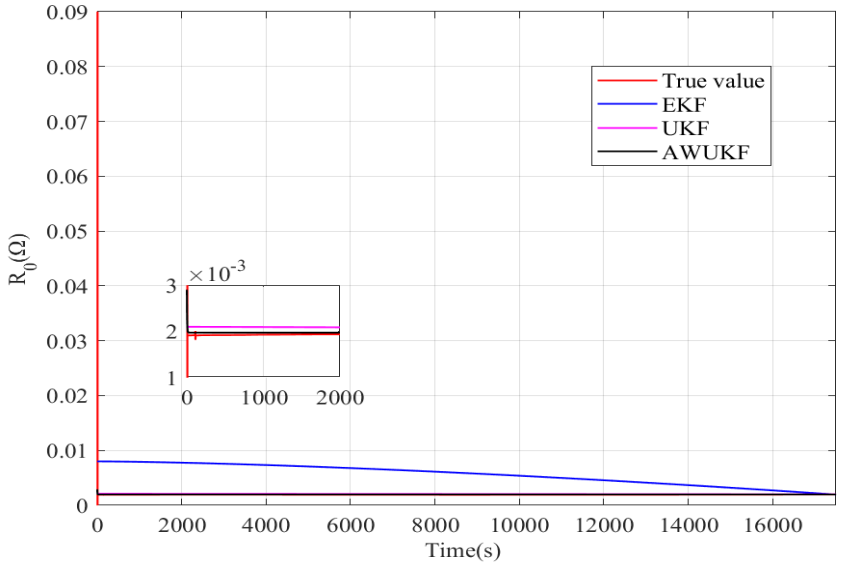

Figure 13. SOH estimation under DST test.

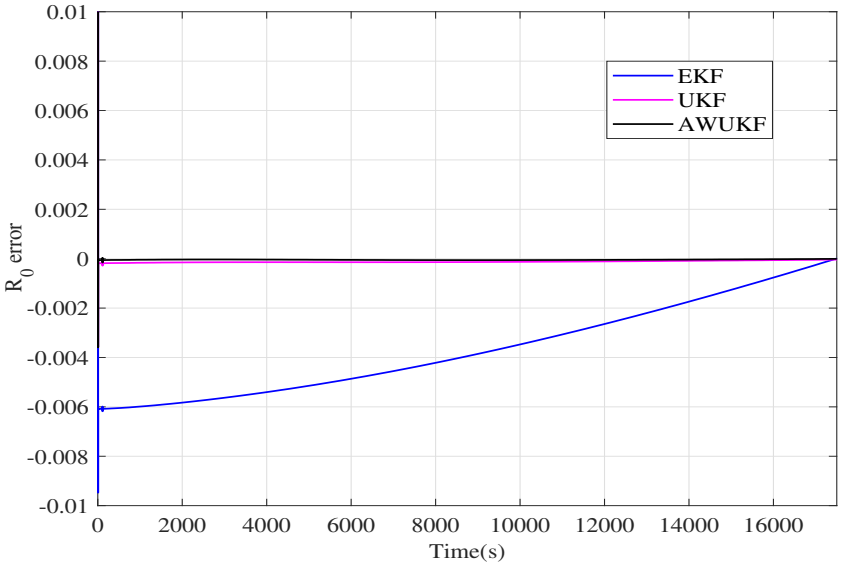

Figure 14. SOH estimation error under DST test.

Figures 15 and 16 show the values of the internal resistance and error curves estimated by each algorithm under FUDS experimental conditions. It can be seen from the figures that the highest error of the AWUKF algorithm is 0.0041, that of the UKF algorithm is 2.15 times higher than the AWUKF algorithm, and that of the EKF algorithm is 4.68 times higher.

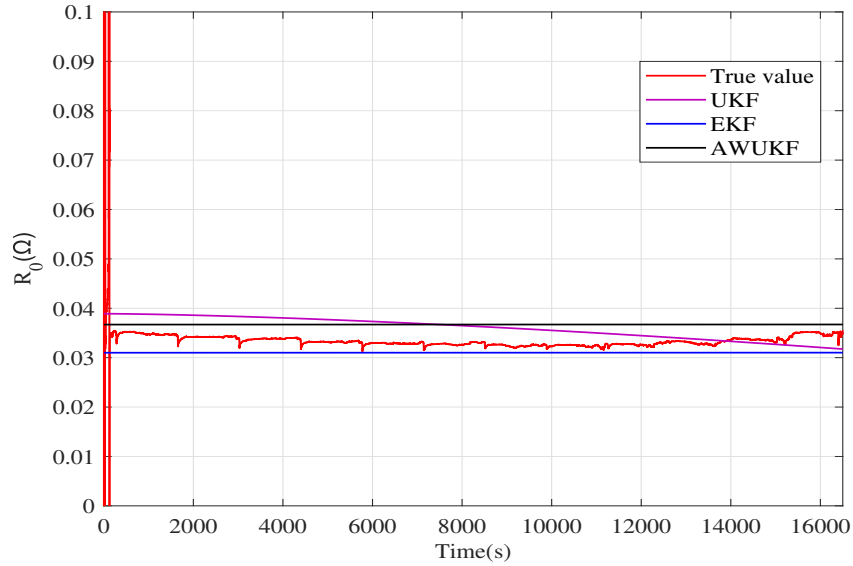

Figure 15. SOH estimation under FUDS test.

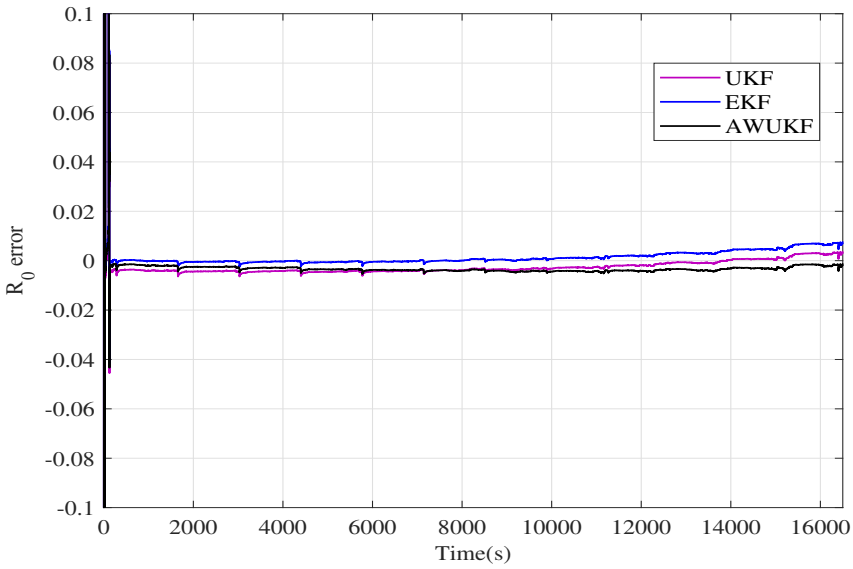

Figure 16. SOH estimation error under FUDS test.

5. Conclusions

In this paper, an equivalent circuit model is adopted to simplify the chemical processes inside lithium batteries. The parameters of lithium batteries are obtained using the MILM algorithm, which provides superior parameter estimation results and lays a foundation for SOC estimation. The AWUKF algorithm is applied to address the sensitivity to noise issue by adaptively adjusting the sigma point weights based on state and measurement residual vectors, which improves the convergence speed of SOC estimation. The simulation indicates that the SOC estimation error of the AWUKF algorithm is below 5.79% for the FUDS experiment and 0.0376 % for the DST experiment. At the same time, the SOH of the battery is estimated using the AWUKF. From the results, we can conclude that the AWUKF algorithm shows faster convergence. In other words, this algorithm has strong applicability under any experimental conditions, and can achieve the detection and estimation of electric vehicles battery properties in real-time.

Author Contributions: Software, C.M.; Formal analysis, Y.J.; Writing—original draft, F.F. All authors have read and agreed to the published version of the manuscript.

Funding: "This research received no external funding.

Data Availability Statement: All data generated or analyzed during this study are included in this article.

Conflicts of Interest: The authors declare no conflict of interest.

References

1. Chen, X.; Bai, Y.K.; Zhao, C.Z.; Shen, X.; Zhang, Q. Lithium bonds in lithium batteries. *Angew. Chem.-Int. Ed.* **2020**, *59*, 11192–11195. [CrossRef] [PubMed]
2. Carkhuff, B.G.; Demirev, P.A.; Srinivasan, R. Impedance-based battery management system for safety monitoring of lithium-ion batteries. *IEEE Trans. Ind. Electron.* **2018**, *65*, 6497–6504. [CrossRef]
3. Kim, J.; Oh, J.; Lee, H. Review on battery thermal management system for electric vehicles. *Appl. Therm. Eng.* **2019**, *149*, 192–212. [CrossRef]
4. Zhang, Z.L.; Cheng, X.; Lu, Z.Y.; Gu, D.J. SOC estimation of lithium-ion battery pack considering balancing current. *IEEE Trans. Power Electron.* **2018**, *33*, 2216–2226. [CrossRef]
5. Zhang, X.Q.; Yan, G.X. Estimating SOC and SOH of lithium battery based on nano material. *Ferroelectrics* **2021**, *580*, 112–128. [CrossRef]
6. Shen, S.Q.; Liu, B.C.; Zhang, K.; Ci, S. Toward fast and accurate SOH prediction for lithium-ion batteries. *IEEE Trans. Energy Convers.* **2021**, *36*, 2036–2046. [CrossRef]
7. Liu, Y.T.; Ma, R.; Pang, S.Z.; Xu, L.C.; Zhao, D.D.; Wei, J.; Huangfu, Y.G.; Gao, F. A nonlinear observer SOC estimation method based on electrochemical model for lithium-ion battery. *IEEE Trans. Ind. Appl.* **2021**, *57*, 1094–1104. [CrossRef]
8. Yuan, C.C.; Wang, B.J.; Zhang, H.Z.; Long, C.; Li, H.H. State-of-charge estimation of lithium-ion battery based on a novel reduced order electrochemical model. *Int. J. Electrochem. Sci.* **2018**, *13*, 1131–1146.
9. Li, W.H.; Demir, I.; Cao, D.C.; Jost, D.; Ringbeck, F.; Junker, M.; Sauer, D.U. Data-driven systematic parameter identification of an electrochemical model for lithium-ion batteries with artificial intelligence. *Energy Storage Mater.* **2022**, *44*, 557–570. [CrossRef]
10. Chen, J.; Ouyang, Q.; Xu, C.F.; Su, H.Y. Neural Network-Based State of Charge Observer Design for Lithium-Ion Batteries. *IEEE Trans. Control Syst. Technol.* **2018**, *26*, 313–320. [CrossRef]
11. Wu, S.L.; Chen, H.C.; Tsai, M.Y. AC Impedance-based Online State-of-charge Estimation for Li-ion Batteries. *Sens. Mater.* **2018**, *30*, 539–550. [CrossRef]
12. Cruz-Manzo, S.; Greenwood, P.; Chen, R. An Impedance Model for EIS Analysis of Nickel Metal Hydride Batteries. *J. Electrochem. Soc.* **2017**, *164*, 1446–1453. [CrossRef]
13. Naseri, F.; Schaltz, E.; Stroe, D.I.; Gismero, A.; Farjah, E. An Enhanced Equivalent Circuit Model With Real-Time Parameter Identification for Battery State-of-Charge Estimation. *IEEE Trans. Ind. Electron.* **2022**, *69*, 3743–3751. [CrossRef]
14. Ma, Y.; Chen, Y.; Zhou, X.W.; Chen, H. Remaining Useful Life Prediction of Lithium-Ion Battery Based on Gauss-Hermite Particle Filter. *IEEE Trans. Control. Syst. Technol.* **2019**, 27, 1788–1795. [CrossRef]
15. Zhang, S.Z.; Guo, X.; Zhang, X.W. Multi-objective decision analysis for data-driven based estimation of battery states: A case study of remaining useful life estimation. *Int. J. Hydrogen Energy* **2020**, *45*, 14156–14173. [CrossRef]
16. Boukouvala, F.; Hasan, M.M.F.; Floudas, C.A. Global optimization of general constrained grey-box models: new method and its application to constrained PDEs for pressure swing adsorption. *J. Glob. Optim.* **2017**, *67*, 3–42. [CrossRef]
17. Zhang, X.; Wang, Y.J.; Liu, C.; Chen, Z.H. A novel approach of battery pack state of health estimation using artificial intelligence optimization algorithm. *J. Power Sources* **2018**, *376*, 191–199. [CrossRef]
18. Liu, D.L.; Wang, S.L.; Fan, Y.C.; Xia, L.L.; Qiu, J.S. A novel fuzzy-extended Kalman filter-ampere-hour (F-EKF-Ah) algorithm based on improved second-order PNGV model to estimate state of charge of lithium-ion batteries. *Int. J. Circuit Theory Appl.* **2022**, *50*, 3811–3826. [CrossRef]
19. Kim, S.; Kim, C. Influence diagnostics in support vector machines. *J. Korean Stat. Soc.* **2020**, *49*, 757–778. [CrossRef]
20. Talha, M.; Asghar, F.; Kim, S.H. A neural network-based robust online SOC and SOH estimation for sealed lead-acid batteries in renewable systems. *Arab. J. Sci. Eng.* **2019**, *44*, 1869–1881. [CrossRef]
21. Tan Y.Q.; Luo, M.J.; She, L.Y.; Cui, X.Y. Joint estimation of ternary lithium-ion battery state of charge and state of power based on dual polarization model. *Int. J. Electrochem. Sci.* **2020**, *15*, 1128–1147. [CrossRef]
22. Li, W.Q.; Yang, Y.; Wang, D.Q.; Yin, S.Q. The multi-innovation extended Kalman filter algorithm for battery SOC estimation. *Ionics* **2020**, *26*, 6145–6156. [CrossRef]
23. El Din, M.S.; Hussein, A.A.; Abdel-Hafez, M.F. Improved battery SOC estimation accuracy using a modified UKF with an adaptive cell model under real EV operating conditions. *IEEE Trans. Transp. Electrif.* **2018**, *4*, 408–417. [CrossRef]
24. Ding, F.; Liu, X.M.; Chen, H.B.; Yao, G.Y. Hierarchical gradient based and hierarchical least squares based iterative parameter identification for CARARMA systems. *Signal Process.* **2014**, *97*, 31–39. [CrossRef]
25. Xu, L. Separable Newton recursive estimation method through system responses based on dynamically discrete measurements with increasing data length. *Int. J. Control Autom. Syst.* **2022**, *20*, 432–443. [CrossRef]

26. Ding, F.; Chen T. Combined parameter and output estimation of dual-rate systems using an auxiliary model. *Automatica* **2004**, *40*, 1739–1748. [CrossRef]
27. Wang, J.; Ji, Y.; Zhang, X. Two-stage gradient-based iterative algorithms for the fractional-order nonlinear systems by using the hierarchical identification principle. *Int. J. Adapt. Control Signal Process.* **2022**, *36*, 1778–1796. [CrossRef]
28. Ding, F.; Chen, T. Parameter estimation of dual-rate stochastic systems by using an output error method. *IEEE Trans. Autom. Control* **2005**, *50*, 1436–1441. [CrossRef]
29. Fan, Y., Liu, X. Two-stage auxiliary model gradient-based iterative algorithm for the input nonlinear controlled autoregressive system with variable-gain nonlinearity. *Int. J. Robust Nonlinear Control* **2020**, *30*, 5492–5509. [CrossRef]
30. Yang, D.; Ding, F. Multi-innovation gradient-based iterative identification methods for feedback nonlinear systems by using the decomposition technique. *Int. J. Robust Nonlinear Control* **2023**, *33*, 7755–7773. [CrossRef]
31. Liu, Q.Y.; Chen F. Model transformation based distributed stochastic gradient algorithm for multivariate output-error systems. *Int. J. Syst. Sci.* **2023**, *54*, 1484–1502. [CrossRef]
32. Yang D, Liu YJ, Ding F, Yang EF. Hierarchical gradient-based iterative parameter estimation algorithms for a nonlinear feedback system based on the hierarchical identification principle. *Circuits Syst. Signal Process.* **2024**, *43*, 124–151. [CrossRef]
33. Liu, X.; Fan, Y. Maximum likelihood extended gradient-based estimation algorithms for the input nonlinear controlled autoregressive moving average system with variable-gain nonlinearity. *Int. J. Robust Nonlinear Control* **2021**, *31*, 4017–4036. [CrossRef]
34. Miao, G.;, Ding, F.; Liu, Q.; Yang, E. Iterative parameter identification algorithms for transformed dynamic rational fraction input-output systems. *J. Comput. Appl. Math.* **2023**, *434*, 115297. [CrossRef]
35. Pan, J.; Liu, S.D.; Shu, J.; Wan, X.K. Hierarchical recursive least squares estimation algorithm for secondorder Volterra nonlinear systems. *Int. J. Control Autom. Syst.* **2022**, *20*, 3940–3950. [CrossRef]
36. Ding, F.; Xu, L.; Zhang, X.; Zhou, Y.H. Filtered auxiliary model recursive generalized extended parameter estimation methods for Box-Jenkins systems by means of the filtering identification idea. *Int. J. Robust Nonlinear Control.* **2023**, *33*, 5510–5535. [CrossRef]
37. Xing, H.; Ding, F.;, Zhang, X.; Luan, X.; Yang, E. Highly-efficient filtered hierarchical identification algorithms for multiple-input multiple-output systems with colored noises. *Syst. Control Lett.* **2024**, *186*, 105762. [CrossRef]
38. Ma, H.; Pan, J.; Ding, W. Partially-coupled least squares based iterative parameter estimation for multi-variable output-error-like autoregressive moving average systems. *IET Control Theory Appl.* **2019**, 13, 3040–3051. [CrossRef]
39. Liu, X.W.; Li, J.; Yao, Z.H.; Wang, Z.Y.; Si, R.C.; Diao, Y.P. Research on battery SOH estimation algorithm of energy storage frequency modulation system. *Energy Rep.* **2021**, *8*, 217–223. [CrossRef]
40. Bavand, A.; Khajehoddin, S.A.; Ardakani, M.; tabesh, a. online estimations of li-ion battery soc and soh applicable to partial charge/discharge. *IEEE Trans. Transp. Electrif.* **2022**, *8*, 3673–3685. [CrossRef]
41. Khayamy, M.; Nasiri, A.; Okoye, O. Development of an Equivalent Circuit for Batteries Based on a Distributed Impedance Network. *IEEE Trans. Veh. Technol.* **2020**, *69*, 6119–6128. [CrossRef]
42. Ji, Y.J.; Qiu, S.L.; Li, G. Simulation of second-order RC equivalent circuit model of lithium battery based on variable resistance and capacitance. *J. Cent. South Univ.* **2020**, *27*, 2606–2613. [CrossRef]
43. Jin, Y.; Zhao, W.C.; Li, Z.X.; Liu, B.L.; Wang, K.S. SOC estimation of lithium-ion battery considering the influence of discharge rate. *Energy Rep.* **2021**, *7*, 1436–1446. [CrossRef]
44. Xie, S.; Chu, X.M.; Liu, C.G.; Liu, J.L.; Mou, J.M. Parameter identification of ship motion model based on multi innovation methods. *J. Mar. Sci. Technol.* **2020**, *25*, 162–184. [CrossRef]
45. Wang, X.Y.; Ma, J.X.; Xiong, W.L. Expectation-maximization algorithm for bilinear state-space models with time-varying delays under non-Gaussian noise. *Int. J. Adapt. Control Signal Process.* **2023**, *37*, 2706–2724. [CrossRef]
46. Zhou, Y.H.; Ding, F. A novel coupled recursive multivariate nonlinear time-series modelling method by using interactive identification. *Appl. Math. Modell.* **2024**, *127*, 571–587. [CrossRef]
47. Gu, Y.; Zhu, Q.; Nouri, H. Identification and U-control of a state-space system with time-delay. *Int. J. Adapt. Control Signal Process.* **2022**, *36*, 138–154. [CrossRef]
48. Li, M.H.; Liu, X.M. The filtering-based maximum likelihood iterative estimation algorithms for a special class of nonlinear systems with autoregressive moving average noise using the hierarchical identification principle. *Int. J. Adapt. Control Signal Process.* **2019**, *33*, 1189–1211. [CrossRef]
49. Zhou, Y.H.;, Ling, K.V. Online network-based identification and its application in satellite attitude control systems. *IEEE Trans. Aerosp. Electron. Syst.* **2023**, *59*, 2530–2543. [CrossRef]
50. Bi, Y.Q.; Ji, Y. Parameter estimation of fractional-order Hammerstein state space system based on the extended Kalman filter. *Int. J. Adapt. Control Signal Process.* **2023**, *37*, 1827–1846. [CrossRef]
51. Li, J.M.; Ding, F.; Hayat, T. A novel nonlinear optimization method for fitting a noisy Gaussian activation function. *Int. J. Adapt. Control Signal Process.* **2022**, *36*, 690–707. [CrossRef]
52. Liu, W.X.; Li, M.H. Unbiased recursive least squares identification methods for a class of nonlinear systems with irregularly missing data. *Int. J. Adapt. Control Signal Process.* **2023**, *37*, 2247–2275. [CrossRef]
53. Xu, L.; Ding, F.;, Zhang, X.; Zhu, Q. Novel parameter estimation method for the systems with colored noises by using the filtering identification idea. *Syst. Control Lett.* **2024**, *186*, 105774. [CrossRef]
54. Pan, J.; Shao, B.; Xiang, J.X.; Zhang, Q. Attitude control of quadrotor UAVs based on adaptive sliding mode. *Int. J. Control Autom. Syst.* **2023**, *21*, 2698–2707. [CrossRef]

55. Xiong, J.; Pan, J.; Chen, G. Sliding mode dual-channel disturbance rejection attitude control for a quadrotor. *IEEE Trans. Ind. Electron.* **2022**, *69*, 10489–10499. [CrossRef]
56. Pan, J.; Chen, Q.; Xiong, J. A novel quadruple boost nine level switched capacitor inverter. *J. Electr. Eng. Technol.* **2023**, *18*, 467–480. [CrossRef]
57. Liao, L.; Yang, D.; Li, X.; Jiang, J.; Wu, T. Fault diagnosis of lithium-ion batteries based on wavelet packet decomposition and Manhattan average distance. *Int. J. Green. Energy* **2024**. [CrossRef]
58. Shu, J.; Wang, S.; Yu, S. CFSA-Net: Efficient large-scale point cloud semantic segmentation based on cross-fusion self-attention. *Comput. Mat. Contin.* **2023**, *77*, 2677–2697. [CrossRef]
59. Chang, Y.F.; Zhou, F.F.; Yan HC, Huang WC, Luo G. Noise and interference suppression control method of DC-DC buck converters based on cascaded filter LADRC. *Int. J. Control Autom. Syst.* **2024**, *22*. [CrossRef]
60. Hao, J.; Zhang, G.S.; Liu, W.Q.; Zheng, Y.Q.; Ren, L. Data-Driven Tracking Control Based on LM and PID Neural Network With Relay Feedback for Discrete Nonlinear Systems. *IEEE Trans. Ind. Electron.* **2021**, *68*, 11587–11597. [CrossRef]
61. Ding, F. Least squares parameter estimation and multi-innovation least squares methods for linear fitting problems from noisy data. *J. Comput. Appl. Math.* **2023**, *426*, 115107. [CrossRef]
62. Xu, L. Parameter estimation for nonlinear functions related to system responses. *Int. J. Control Autom. Syst.* **2023**, *21*, 1780–1792. [CrossRef]
63. Xu, L. Separable multi-innovation Newton iterative modeling algorithm for multi-frequency signals based on the sliding measurement window. *Circuits Syst. Signal Process.* **2022**, *41*, 805–830. [CrossRef]
64. Fan, Y.M.; Liu, X.M. Auxiliary model-based multi-innovation recursive identification algorithms for an input nonlinear controlled autoregressive moving average system with variable-gain nonlinearity. *Int. J. Adapt. Control Signal Process.* **2022**, *36*, 521–540. [CrossRef]
65. Hu, C.; Ji, Y.; Ma, C.Q. Joint two-stage multi-innovation recursive least squares parameter and fractional-order estimation algorithm for the fractional-order input nonlinear output-error autoregressive model. *Int. J. Adapt. Control Signal Process.* **2023**, *37*, 1650–1670. [CrossRef]
66. Pan, J.; Liu, Y.Q.; Shu, J. Gradient-based parameter estimation for an exponential nonlinear autoregressive time-series model by using the multi-innovation. *Int. J. Control Autom. Syst.* **2023**, *21*, 140–150. [CrossRef]
67. Pan, J.; Zhang, H.; Guo, H.; Liu, S.; Liu, Y. Multivariable CAR-like system identification with multi-innovation gradient and least squares algorithms. *Int. J. Control Autom. Syst.* **2023**, *21*, 1455–1464. [CrossRef]
68. Wan, L.J.; Ding, F. Decomposition- and gradient-based iterative identification algorithms for multivariable systems using the multi-innovation theory. *Circuits Syst. Signal Process.* **2019**, *38*, 2971–2991. [CrossRef]
69. An, S.; He, Y.;, Wang, L.J. Maximum likelihood based multi-innovation stochastic gradient identification algorithms for bilinear stochastic systems with ARMA noise. *Int. J. Adapt. Control Signal Process.* **2023**, *37*, 2690–2705. [CrossRef]
70. Xu, L.; Xu, H.; Ding, F. Adaptive multi-innovation gradient identification algorithms for a controlled autoregressive autoregressive moving average model. *Circuits Syst. Signal Process.* **2024**, *43*. [CrossRef]
71. Chen, J.; Pu, Y.; Guo, L.X.; Cao, J.F.; Zhu, Q.M. Second-order optimization methods for time-delay autoregressive exogenous models: Nature gradient descent method and its two modified methods. *Int. J. Adapt. Control Signal Process.* **2023**, *37*, 211–223. [CrossRef]
72. Ding, F.;, Xu, L.; Zhang, X.; Ma, H. Hierarchical gradient- and least-squares-based iterative estimation algorithms for input-nonlinear output-error systems by using the over-parameterization. *Int. J. Robust Nonlinear Control* **2024**, *34*, 1120–1147. [CrossRef]
73. Ding, F.; Shao, X.; Xu, L.; Zhang, X.; Xu, H.; Zhou, Y. Filtered generalized iterative parameter identification for equation-error autoregressive models based on the filtering identification idea. *Int. J. Adapt. Control Signal Process.* **2024**, *38*, 1363–1385. [CrossRef]
74. Gu, Y.; Dai, W.; Zhu, Q.M.; Nouri, H. Hierarchical multi-innovation stochastic gradient identification algorithm for estimating a bilinear state-space model with moving average noise. *J. Comput. Appl. Math.* **2023**, *420*, 114794. [CrossRef]
75. Pan, J.; Jiang, X.; Wan, X.K.; Ding, W. A filtering based multi-innovation extended stochastic gradient algorithm for multivariable control systems. *Int. J. Control Autom. Syst.* **2017**, *15*, 1189–1197. [CrossRef]
76. Xu, L.; Ding, F. Decomposition and composition modeling algorithms for control systems with colored noises. *Int. J. Adapt. Control Signal Process.* **2024**, *38*, 255–278. [CrossRef]
77. Liu, S.Y., Wang, Y.J. Joint iterative state and parameter estimation for bilinear systems with autoregressive noises via the data filtering. *ISA Trans.* **2024**, *147*, 337–349. [CrossRef] [PubMed]
78. Ding, F.; Ma, H.; Pan, J.; Yang, E.F. Hierarchical gradient- and least squares-based iterative algorithms for input nonlinear output-error systems using the key term separation. *J. Frankl. Inst.* **2021**, *358*, 5113–5135. [CrossRef]
79. Xing, H.M.; Ding, F.; Pan, F.; Yang, E.F. Hierarchical recursive least squares parameter estimation methods for multiple-input multiple-output systems by using the auxiliary models. *Int. J. Adapt. Control Signal Process.* **2023**, *37*, 2983–3007. [CrossRef]
80. Pan, J.; Li, W.; Zhang, H.P. Control algorithms of magnetic suspension systems based on the improved double exponential reaching law of sliding mode control. *Int. J. Control Autom. Syst.* **2018**, *16*, 2878–2887. [CrossRef]

81. Ding, F.; Xu, L.; Zhang, X.; Zhou, Y.; Luan, X. Recursive identification methods for general stochastic systems with colored noises by using the hierarchical identification principle and the filtering identification idea. *Annu. Rev. Control* **2024**, *57*, 100942. [CrossRef]
82. Ji, Y.; Kang, Z.; Zhang, X.; Xu, L. Model recovery for multi-input signal-output nonlinear systems based on the compressed sensing recovery theory. *J. Frankl. Inst.* **2022**, *359*, 2317–2339. [CrossRef]